Liquid crystalline phase transitions in confined geometries

S. Krishna Prasad, D.S. Shankar Rao AND Geetha G. Nair

Abstract | Investigations on liquid crystals confined in restricted geometries have been attracting significant attention in the past few years. The voids in the confining matrix could be highly regular as in the case of membranes like Anopore, Nuclepore, etc. or an irregular network like in the case of aerogels. Here we describe the results of our recent experimental investigations on different phase transitions when the liquid crystal is confined in the voids of the Anopore membranes. Examples discussed involve melting in lower dimensions and paraelectric to ferroelectric transitions.

1. Introduction

Understanding the behaviour of finite sized systems is important in many areas of physics from both theoretical and experimental points of view. In particular, the influence of the size of the system on phase transitions has received interest for more than a century, although there is a lot of activity in the past two decades. For example, the effects of confinement on freezing and melting transitions have been exhaustively studied[1–3]. The interest in this phenomenon is owing to the fact that such studies have raised fundamental questions, challenging the known static and dynamic behaviours. Understanding these phenomena is not only interesting from basic science point of view, but necessary for many industrial and geophysical operations, like pollution control, mixture separation, catalysis, lubrication, adhesion, tertiary oil recovery, gas field technology, removal of pollutants from ground water and soils, fabrication of nanomaterials, etc. From a conceptual point of view, the differences between the bulk and the confined systems arise from the overlap and competition between the typical correlation lengths driving the phase structure or dynamics, and the finite size of the system. These boundaries define an interface, with another physical state that may manifest as an external field. The introduction of a natural length to the system by the confining geometry can cause two major effects: the first is the cut-off or finite size effect, owing to which neither the static nor the dynamic correlation length can grow larger than the maximum pore size. Such a constraint may result in the breakdown of scaling and universality[4,5]. The second is the surface effect, caused by the enhancement in the surface-to-volume ratio due to the additional surface of the confining medium[2,6,7].

Liquid crystals are especially suitable for work on confined geometries because (i) they exhibit a variety of phases with different degrees of orientational or translational order, (ii) the involved transitions are second-order or at best weakly first-order, (iii) they are typical representatives of soft (elastically weak) materials, (iv) their response to perturbations induced by the confining matrix is pronounced and long ranged, (v) they do not have chemical interactions with the typical host matrix and owing to (vi) strong competition among elastic, surface, and external field forces. Not surprisingly investigations on liquid crystals confined in restricted geometries have been attracting significant attention[8–16]. Apart from simply confining the sample in wedge-shaped cell, pre-fabricated geometries such as

Centre for Liquid Crystal Research, Jalahalli, Bangalore 560013
skpras@gmail.com

Figure 1: Schematic diagram of the pore structure of an Anopore membrane

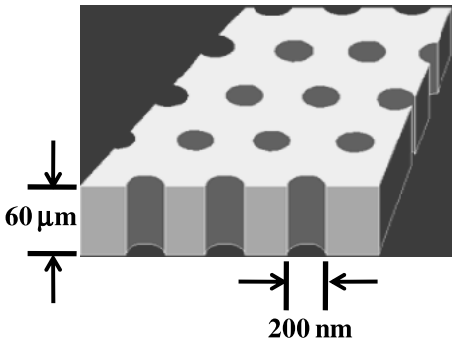

porous membranes and in-situ fabricated network confinements employing particles capable of forming hydrogen bonding such as aerosil, etc have been employed for these studies. In the case of the pre-fabricated systems, the voids in the confining matrix could be highly regular as in the case of membranes like Anopore, Nuclepore, etc. or an irregular network like in the case of aerogels. The geometrically enforced disorder observed in these situations can also be realized by including or "filling" certain particles into the liquid crystal (LC). A popular choice for the particle has been aerosil: silica spheres of ∼7 nm diameter whose surfaces are decorated to achieve hydrophilic or hydrophobic interactions which result in *in-situ* created voids for confining the liquid crystalline medium. In this article we summarise the results of our recent experimental investigations on different phase transitions when the liquid crystal is confined in pre-fabricated geometries using the Anopore membrane.

The Anopore membranes are made from an inorganic aluminium oxide matrix using an electrochemical anodizing process in which the anodizing voltage controls the pore size. Since the process is electrochemical, conditions can be precisely controlled and a reproducible pore structure with narrow pore size distribution and high pore density is obtained. A schematic diagram of the pore structure of an Anopore membrane is shown in figure 1. The cross-section shows uniform cylindrical channels despite the 'honeycomb' nature of the surface. The inner cavity walls are smooth and easily accessible to chemical treatments. These membranes are commercially available from Whatman Corp., USA under the trade name Anodisc with a diameter of 13 mm and pore size 0.2 μm having 50% porosity and density of pores as 10^9 cm^{-2}.

Keeping the broad readership in mind we provide in the following a brief description of the liquid crystalline phases [See e.g., Ref. 17] discussed in this article. The simplest of the liquid crystalline phases is the nematic (N), which can be termed as an orientationally ordered fluid (Figure 2b). This phase is characterized by a preferred molecular orientation direction labeled the director **n**, and no positional order. Introducing a one-dimensional positional order along the director direction, results in the formation of the smectic phases. To be more precise, such a phase will have a layered structure possessing quasi-long-range positional order in one dimension represented by a mass-density wave. The wave vector of this density wave is along the director in the case of the smectic A (SmA) phase (Figure 2c), while it is tilted in the case of the smectic C (SmC) phase (Figure 2d). If the constituent molecules are chiral then a helix can also be present along the layer normal direction in the chiral smectic C (SmC*) phase (Figure 2f). Lowering the symmetry of the system further, one comes across the hexatic phase, which has short range positional ordering within the layers (just as for smectics) but long range "bond-orientational order" [The bond here does not refer to a chemical one but of the geometrical variety. The bonds describe lines that join the centres of mass of nearest neighbor molecules]. Here again both the orthogonal (referred to as hexatic B or HexB, see Figure 2h) and tilted varieties are seen. For historic reasons studies on soft crystal phases such as the crystal B (CrB, Figure 2i), possessing long range positional ordering along all the three directions is also part of liquid crystal research. This phase is actually a plastic crystal: although possessing a three dimensional (3D) positional order the molecules still retain the rotational degree of freedom. Stated otherwise this means that the smectic layers can slide past each other. All these phases exist between a true crystal (Cr, Figure 2e) and the isotropic liquid (I, Figure 2a).

This review is limited to our work[11–14] on phase transitions that involve the SmA as one of the phases.

Figure 2: Schematic arrangement of the molecules in the different liquid crystalline phases described in this article: (a) isotropic, (b) nematic, (c) smectic A, (d) smectic C and (e) crystalline phases. The helix formed in the smectic C phase consisting of chiral molecules is shown in (f). The appearance of the bond orientational order with short range positional order in the layer plane of the hexatic B phase is shown in (h), and the additional long range positional order developed in the soft crystal (crystal B) is depicted in (i). For comparison the liquid-like order within the layer plane of the smectic A phase is given in (g).

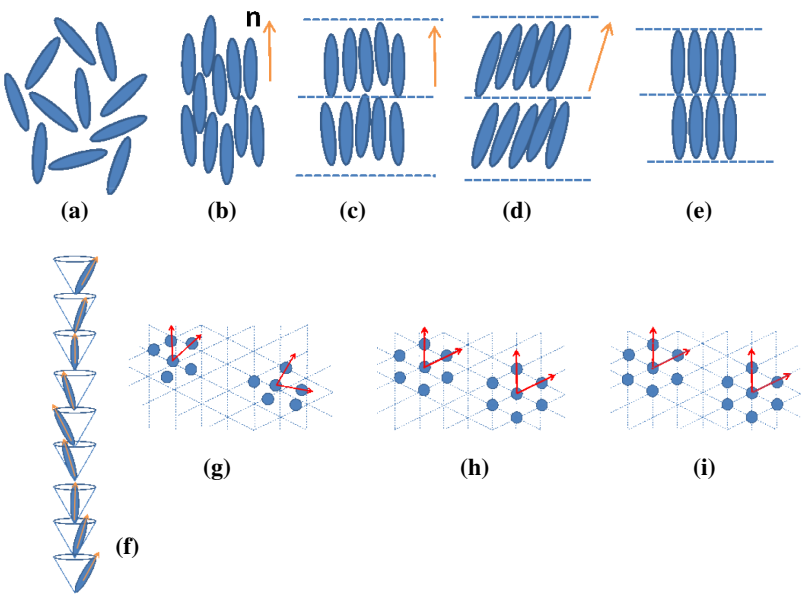

The different cases correspond to the other phase being CrB, HexB, chiral and achiral SmC phases. Note that the transformations to the SmA from the CrB and the HexB phases are considered to be melting transitions, but quite different from the normal solid–liquid melting. The one involving CrB phase is a 2D melting transition and that with the HexB, a unique melting of the bond orientational order. The molecular structures of the compounds mentioned in this article are shown in Table 1.

2. SmA-CrB transition

The DSC scans in the bulk and the Anopore configurations for the compound 4O.8 obtained with a heating rate of 5 °C/min are shown in Figure 3. In comparison to the N-I and Sm A-Cr B transitions, the Sm A-N transition has a very small thermal contribution. This feature in conjunction with the larger noise factor seen for the Anopore samples makes it difficult to identify the Sm A-N transition in the confined system. Comparing the N-I transition peak for the bulk and Anopore samples it is seen that the peak height gets reduced considerably (by a factor of 18) for the Anopore sample. Upon confinement in the membranes, the transition temperature as well as the transition enthalpy (ΔH) shows an appreciable decrease. Very similar features are seen for the SmA-CrB transition with ΔH dropping by as much as 30% for the Anopore system.

The frequency dependence of the dielectric spectrum (C'' vs f, where $C'' = C' * D$, D being the dielectric loss and C', the sample capacitance) was analysed using the Havriliak-Negami (HN) equation with an additional term to account for the DC conductivity. The representative dielectric spectra for the bulk sample in the SmA and CrB phases, as well as in the transition region are shown in figure 4 (left panels). In the CrB and SmA phases the peak is sharp whereas in the coexistence (transition) region the peak is substantially broad. Interestingly, the data in the coexisting region is well described by two HN profiles bringing out the presence of the coexisting peaks. Such a feature, rarely observed in dielectric measurements, is indeed in conformity with the DSC data (mentioned above) that exhibits a first order character. In contrast, Anopore samples exhibit a single relaxation in the two phases as well as in the transition region (see Figure 4, right panels). This is in agreement with the weakening of the transition upon confinement, as seen in the DSC scans. A feature seen in the fitting of the C' vs. f data to the HN equation is that whereas for the bulk sample the relaxation is nearly a perfect Debye

Table 1: Molecular structures of the compounds mentioned in this article

Compound	Structure
4O.8	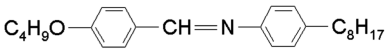
46OBC	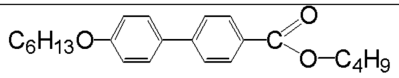
A7	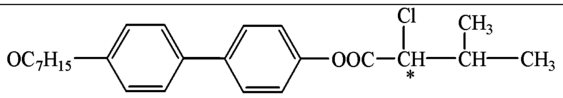
TCOB	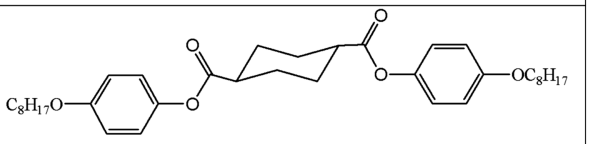
8OSI*	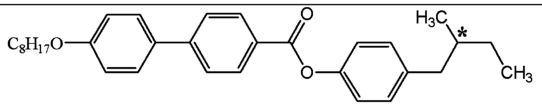

Figure 3: Differential Scanning Calorimetric (DSC) profiles for the (a) bulk and (b) Anopore samples in the heating mode showing clear thermal anomalies at the I-N, N-SmA and SmA-CrB transitions of the compound 4O.8. For ease of comparison, the scale on the vertical axis is kept the same in both the cases and to facilitate this, the raw data for the Anopore sample has been multiplied by a factor of 22.

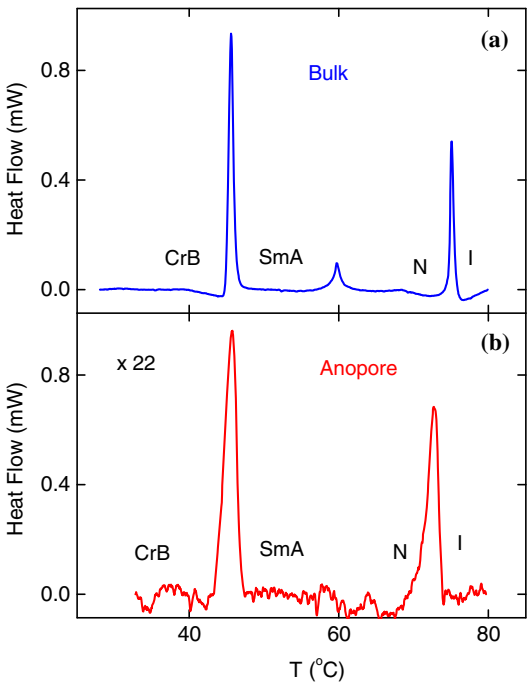

curve with a single relaxation time, in the Anopore the deviation from such a description, which is temperature dependent, is upto 15%.

The temperature dependence of the relaxation frequency f_R in the vicinity of the SmA-CrB transition for the bulk and Anopore are presented

Figure 4: Representative loss (C″) curves for the bulk (a-c) and Anopore (d-f) samples in the SmA and CrB phases as well as the transition region. The circles represent the experimental data and the blue line, the fit to the HN equation plus terms to account for conductivity and cell relaxation contributions (shown as red and green dashed lines respectively in panel (a)). The black line stands for the dielectric relaxation of interest. Unlike in the case of the Anopore sample, the transition region for the bulk sample is marked by a coexistence of contributions (shown as red and green solid lines in panel (b)) from the two phases across the transition.

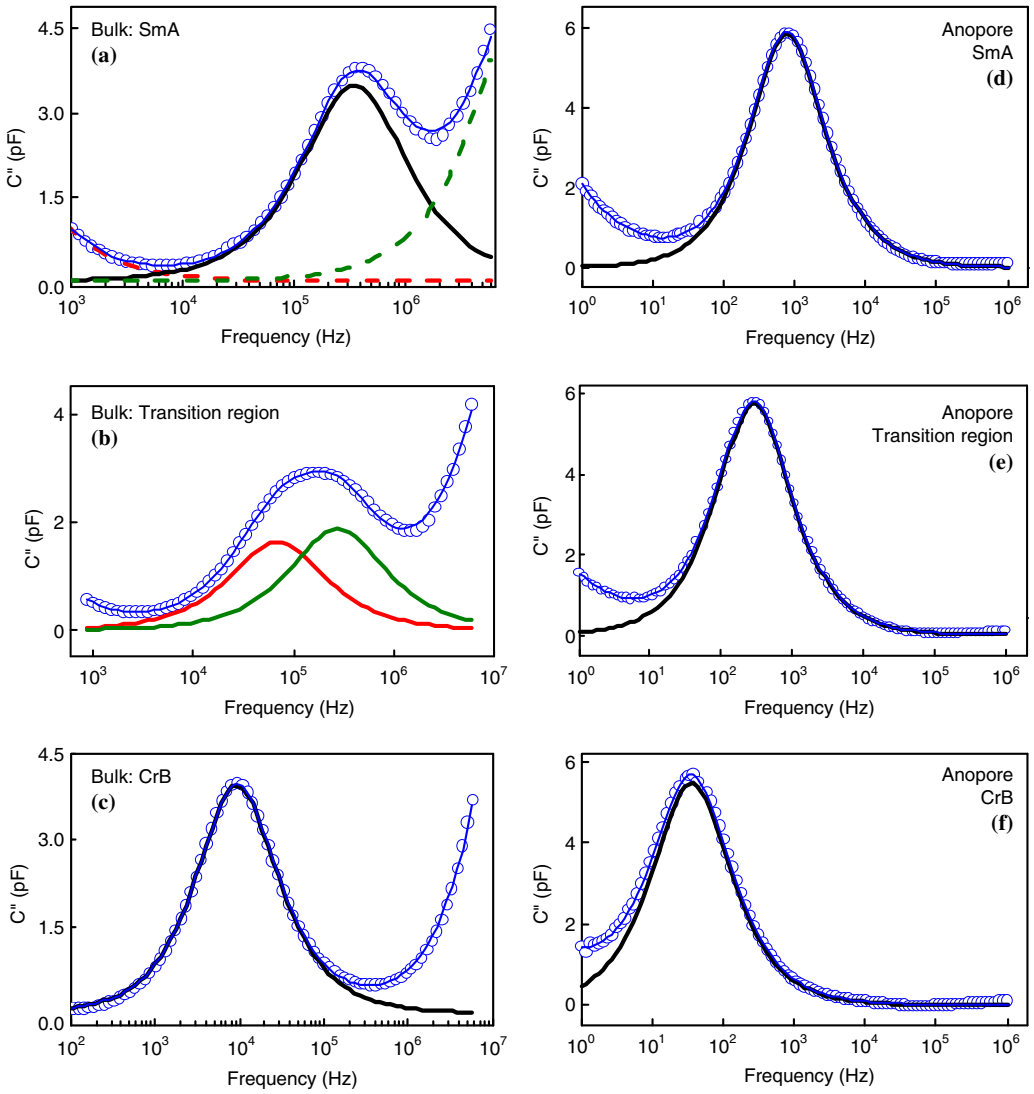

in Figure 5. The observed dependences are very different for the sample confined in Anopore membrane, in comparison with that for the bulk sample. For the bulk sample, the decrease in the value of f_R at the transition is abrupt, as is expected for a first order transition. Further, as the sample transforms from the SmA to the CrB phase there is an increased two dimensional ordering of the centres of molecules within the CrB layers which leads to a greater restriction of the orientational fluctuation of the long molecular axes compared to that in the SmA phase resulting in a substantial lowering of f_R at the transition. Other features such as the absence of any pre- or post-transitional behavior, smooth crossover in the transition region of the dielectric strength of the contributions from the two phases, clearly demonstrate the fact that as the regions with, say CrB ordering, grow at the expense of those with SmA ordering, so does the relevant dielectric contribution.

For the sample in the Anopore membrane, the decrease in the value of f_R across the SmA-CrB transition is still appreciable, but the change is gradual unlike that for the bulk sample, owing to as

Figure 5: Semi-logarithmic plots of f_R versus inverse temperature for the bulk (blue circles), and Anopore (red cirlces) samples. The lines drawn represent fits to an Arrhenius equation by considering data outside the transition region. [The axes on the top and the right are for the bulk sample and those on the left and bottom are for the Anopore sample.] The data in the vicinity of the transition region (shaded rectangle) for the bulk sample, shown on an enlarged scale at the top, demonstrates the coexistence of relaxations from the two phases.

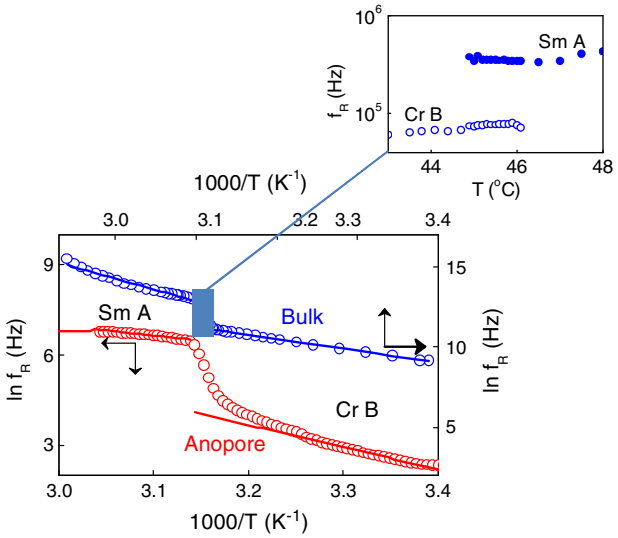

has already been commented on, widening of the transition. Confinement of the material in pores results in a reduction of f_R by about three orders of magnitude when compared with the values for the bulk sample. Unlike the bulk sample, the data for the membranes show more temperature dependence in the CrB phase than in the SmA phase. For the bulk sample, Arrehenius type behaviour is seen throughout the two mesophases. In contrast, for Anopore, such a trend is observed in the entire range of the SmA phase, but only well away from the transition in the CrB phase, again in line with the weakening of the transition.

3. SmA-HexB transition

Figure 6 shows DSC scans for the sample 46OBC in the bulk and Anopore configurations for a range of heating rates. Broadening and reduction in the height of the peaks, upon confinement, are seen in this case also. The transition enthalpy values show a monotonic decrease with decreasing rates employed. The value extrapolated to zero heating rate is negligibly small, indicating the second order nature of the transition in both bulk and the Anopore samples. The transition temperature (T_c) has a strong dependence on the heating rate for the Anopore sample unlike in the bulk case (see insets in figure 6). The diffraction patterns obtained in the low angle region in the SmA and HexB phases of the bulk and Anopore samples are shown in Figure 7.

The most significant feature to be noted in both the phases is the presence of multiple reflections, which turn out to be the higher-order harmonic reflections of the fundamental. The observation of the strong higher harmonic peaks is rather surprising, since it is well known that smectic layering can be described by a pure sinusoidal wave and therefore the higher order harmonic reflections from the layering, even if present, should be extremely weak, as is seen for the smectic phase almost as a rule. For example, earlier reports[18] have shown that the intensity of the second harmonic reflection is about 10^4 times weaker compared to that for the fundamental. Thus, in present case the second harmonic is 200 times stronger than commonly observed. The second harmonic is seen even after confinement, although with a reduced strength. It may be mentioned here that harmonic reflections with sufficient intensity are generally observed in dimeric materials having two aromatic mesogenic units attached through a flexible aliphatic "spacer" chain, wherein the mutual dislike between the aromatic and the aliphatic parts present in the terminal as well as spacer units can reduce the layer undulation causing the layering to be much well defined than in other compounds. Such a behaviour is also seen in antiferroelectric phase of chiral materials and bilayer smectic A phase of terminally polar molecules, owing to dipolar contributions, and sugar-based materials due to the intermolecular hydrogen bonding. The lamellar

Figure 6: DSC scans across the SmA-HexB transition of 46OBC in the (a) bulk and (b) Anopore configuration for different heating rates. The peak heights are seen to be strongly dependent on the rate of heating in both the cases. For the bulk sample, the peak temperature T_c, taken as the transition temperature increases slightly with increasing rate, a feature shown as a grey line in the main panel and separately as an inset in (a). In contrast, in the Anopore sample T_c depends strongly on the rate employed.

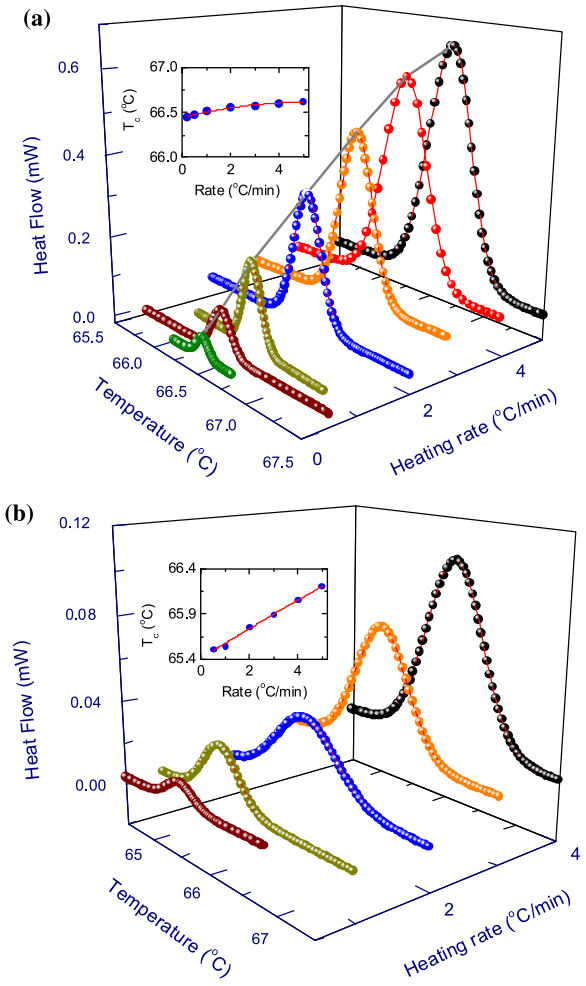

L_α phase of lyotropic systems also exhibits such a feature owing to the well defined segregation of the layers caused by the presence of sheets of water. The thermal variation of I_{100}, the intensity of the fundamental reflections as well as I_{200}/I_{100}, the ratio of the intensities of the second harmonic to the fundamental, for both the bulk and the Anopore samples are shown in the figure 8 (a) and (b). For both the samples, the transition point is clearly marked by a substantial increase in I_{100}, although the increase appears gradual for the Anopore sample. The harmonic intensity ratios also show about 30% increase when the material transforms from the SmA to the HexB phase. Note that the molecules lie perpendicular to the walls of the pores. Since the layer spacing is about 25 Å and the pore diameter is 200 nm, only about 80 layers can be accommodated inside a pore. This restriction may cause the magnitude of the layering to be altered and consequently diminish the intensity of the I_{200} reflection in comparison to that of I_{100}. A possible reason for the observation of strong harmonics for this compound is the short range herringbone order that could be present due to the phase immediately below the HexB and possessing such an order, which would diminish the smectic fluctuations. The temperature variation of the layer spacing d for the bulk and Anopore samples (figure 8(c)) shows qualitatively similar behaviour. However, the absolute values as well as the overall increase are slightly larger for the Anopore sample, perhaps due to a stretching of the alkyl chains caused by the

Figure 7: Diffraction patterns in the low-angle region of the HexB phase (right panels) and SmA phase (left panels) of the bulk and Anopore samples. The feature to be noted particularly is the presence of higher harmonic reflections.

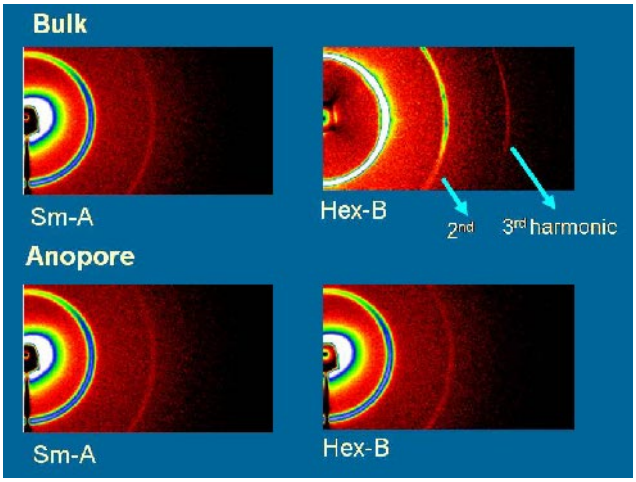

larger surface to volume ratio of the membranes. Further, at the transition, the layer spacing increases at a much slower rate for the Anopore sample than for the bulk, in agreement with the DSC result that the transition is weaker for the Anopore sample.

Both the SmA and HexB phases have a liquid-like ordering of the molecules in the layer plane. However, the onset of the hexatic order results in a significant increase in the in-plane density as well as the in-plane positional correlations. Experimentally, this manifests as a diffraction peak in the wide angle region which is broad and diffuse in both the phases, but relatively sharper in the HexB phase than the SmA phase. The temperature dependences of the parameters Q_o, the wave vector of the peak position (corresponding to the in-plane density), and κ, the associated half width (inversely proportional to the in-plane positional correlation) of the wide-angle diffraction profiles are given in Figure 9. The wave vector data can be quantitatively analyzed in terms of the expression given by the theory of Aeppli and Bruinsma[19]. For example, the expression for the wavevector is

$$Q_o(t) = Q_c[1 \mp A^{\pm} t^{1-\alpha}] \qquad (1)$$

Here Q_c is a constant, $t[=(T-T_c)/T_c$, T_c being the SmA-HexB transition temperature] is the reduced temperature, α is the exponent, and A^+/A^-, the amplitude ratio. To be emphasized is the point that the exponent α is the same as the one which describes the behaviour of the specific heat across the transition. The solid lines in figure 9(a) show the fit obtained for the bulk and Anopore samples and yield $A^+/A^- = 1.89 \pm 0.08$; 1.73 ± 0.13, and $\alpha = 0.47 \pm 0.01$; 0.50 ± 0.01 for the two samples respectively. [The values for the bulk are in close agreement with those reported from x-ray and specific heat, see Ref. 20]. Another aspect to be noted is that while in the SmA phase the κ values are comparable for the bulk and Anopore samples, the limiting value of κ in the HexB is about 30% higher for the Anopore sample. This suggests that the confinement of the sample into the porous matrix reduces the in-plane correlation, a feature that is not surprising considering the influence of the finite size effects and the length scales of the system: diameter of the pores (~2000 Å), and the correlation lengths in the SmA (~20 Å) and HexB (~160 Å).

4. SmA-SmC transition

In this section we consider two samples, A7 and TCOB, as representatives exhibiting different aspects of the SmA-SmC transition. In the bulk, A7 exhibits a first order transition, a recent finding for this phase transformation. TCOB, on the other hand, has been chosen as it exhibits the de Vries type of SmA phase. (Smectic A phase in which there is no global correlation of the tilting direction of the molecules, is labelled de Vries SmA phase; this phase has attracted attention owing to its importance for improving device characteristics[21]). While A7 is also chiral in nature (for this reason the SmC phase exhibited by them is labelled SmC*), TCOB is not.

4.1. *A7*

DSC scans obtained with the bulk and Anopore samples while cooling the sample at a rate of

Figure 8: Temperature dependence of (a) I_{100}, the peak intensity of the fundamental low-angle reflection, (b) the ratio of the intensities of the second harmonic to the fundamental reflection (I_{200}/I_{100}) and (c) the smectic layer thickness across the SmA-HexB transition of 4OOBC in the bulk (the blue data set) and Anopore (the red data set) configurations. In all the cases the onset of the transition to the HexB phase is marked by an increase in the corresponding parameter, although more gradually for the confined situation.

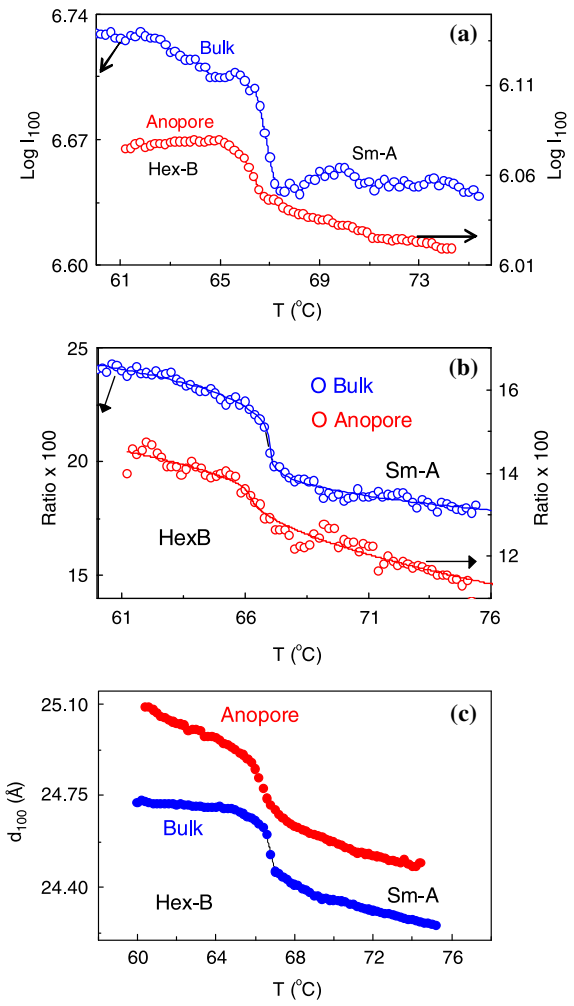

5 °C/min are shown in Figure 10. The four peaks seen for the bulk sample correspond to the I-SmA, SmA-SmC*, SmC*-Cr G and Cr G-Cr H transitions. The profiles as well as the transition enthalpies confirm the first order character of all the transitions, more importantly the SmA- SmC* transformation. The scan for the Anopore sample looks qualitatively similar, and therefore we presume that it has the same phase sequence as that of the bulk sample. X-ray studies, to be described below, corroborate this argument. The confinement of the sample in the membrane, however, introduces some differences. First, it broadens the transitions, by a factor of 3.6, 6.7, 1.8 and 1.4 times for I-Sm A, SmA-SmC*, SmC*-Cr G and Cr G-Cr H transitions, respectively. Second, the peak height is reduced and rounded for all the transitions, especially so for the SmA-SmC* transition with one order of magnitude reduction in the peak height (inset of Figure 10). In fact, the signal due to this transition becomes quite weak and difficult to locate with slower cooling rates. Confinement-induced shift in the transition temperatures is also observed: while the I-SmA transition shows a small (0.2 °C) upward shift, the temperatures for the other transitions are lower in the Anopore sample. The largest shift seen is for the SmC*- CrG transition with a temperature shift of 2.5 °C; this results in an increase in the temperature range of the SmC* phase from 2.2 °C in the bulk to 4 °C in the Anopore sample. As

Figure 9: (a) Thermal variation of the wave vector Q_o of the wide-angle reflection in the bulk and Anopore samples. The solid lines are fits done to eq. (1); the best fit values of the exponent α are 0.47 ± 0.01 and 0.50 ± 0.01 for the bulk and confined cases respectively. (b) Temperature dependence of the half width of the wide-angle reflection in bulk and Anopore samples. The reciprocal of κ is directly proportional to the correlation length of the in-plane positional order. The solid line in both sets of data is only a guide to the eye.

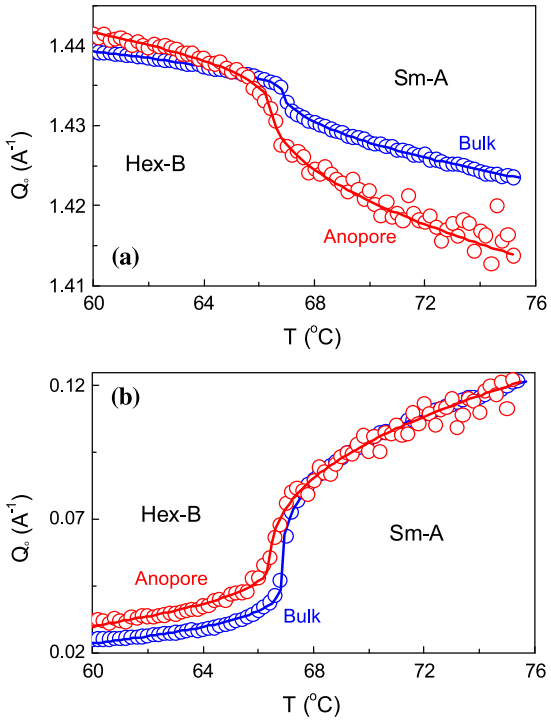

Figure 10: Differential scanning calorimetric scan in the cooling mode (rate 5 °C/min) in the bulk and the confined geometries for the sample A7. Note that for all the transitions the peak width is more and the peak height is lower for the Anopore sample than for the bulk sample. The data in the vicinity of the SmA–SmC* transition for the Anopore sample is shown on an enlarged scale in the inset. CrG and CrH phases are the tilted analogues of the soft crystal CrB mentioned above; the CrH phase possesses a herringbone order, in addition.

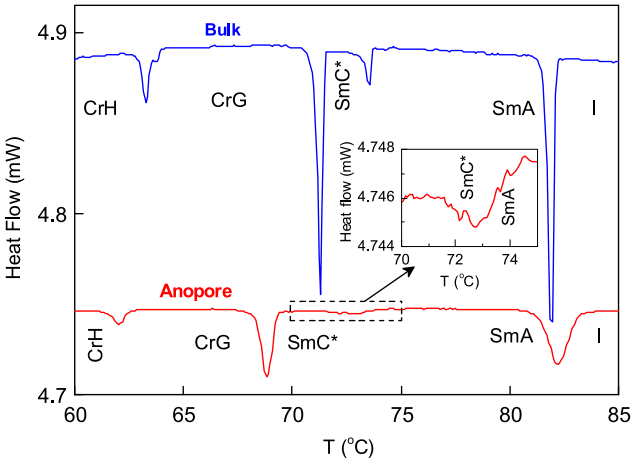

Figure 11: Thermal variation of the layer spacing for the (a) bulk and (b) Anopore samples near the SmA–SmC* transition of the compound A7. While the Anopore sample shows a smooth variation, the bulk sample exhibits an abrupt change across the transition, known to be first order for this material. The temperature dependence of the molecular tilt angle determined from the layer spacing data is shown in the inset; while for the bulk sample the line through the data points is only a guide to the eye, in the Anopore case it represents the fit done to the extended mean field model, eq. (3).

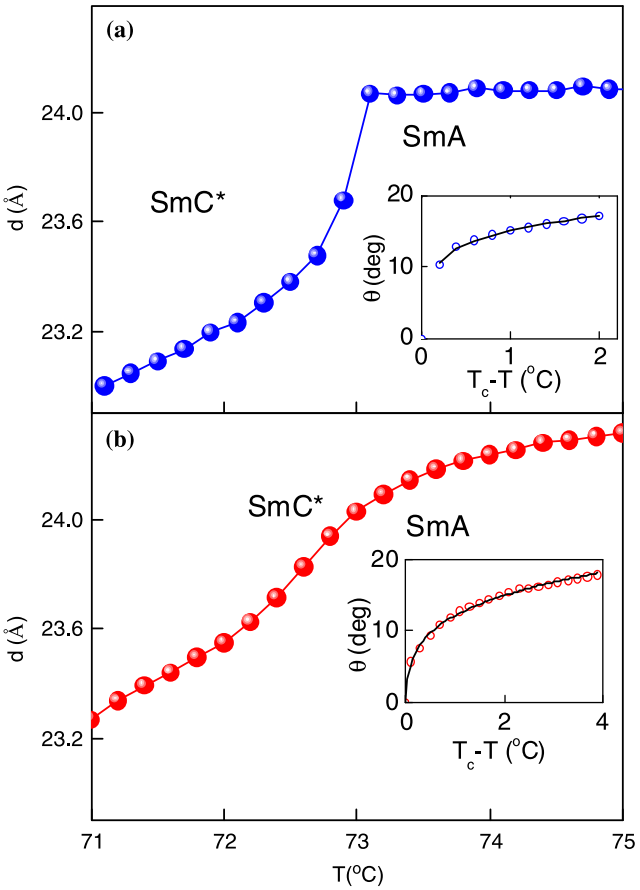

Table 2: Mean field parameters t_o, R and b/a extracted from eq.3

Compound	Configuration	t_o	R	b/a (rad^{-2} K)
8OSI*	Bulk	.0002	.006	.011
	Anopore	.008	.04	.07
A7	Bulk	First order transition		
	Anopore	.003	.037	.027

discussed earlier, these features are generally seen in restricted geometries.

The temperature variation of the layer spacing (d) in the bulk and Anopore samples in the vicinity of the SmA-SmC* transition is shown in Figures 11 (a) and (b), respectively. For the bulk sample, there is an abrupt variation of 0.4 Å in d across the transition, as is indeed expected due to its first order character. In contrast to the behaviour in the bulk, the Anopore sample shows a smooth variation through the transition. As already noted in the case of the SmA-HexB transition, the d value is slightly larger for the Anopore sample than for the bulk, perhaps due to a slight stretching of the alkyl chains caused by the suppression of thermal fluctuation in the confined geometry. The tilt angle θ is the additional order parameter for the SmC* phase in comparison to the SmA phase. With the Xray data and assuming that the molecules tilt as a rigid rod the tilt angle can be calculated using $\theta = \cos^{-1}(d_{\mathrm{SmC}^*}/d_{\mathrm{SmA}})$. The thermal variation of θ thus calculated for the bulk and Anopore samples are shown in the insets of Figures 11 (a) and (b). In contrast to the jump in θ seen at the transition for the bulk sample, the Anopore sample shows a much smoother variation. According to the generalized mean field model[22], the free energy for the SmC*-SmA transition can be written as

$$F = F_0 + \frac{1}{2}at\theta^2 + \frac{1}{4}b\theta^2 + \frac{1}{6}c\theta^6 \qquad (2)$$

where F_o is the background part, $t[=(T-T_c)/T_c]$ is the reduced temperature and a,b,c are temperature independent coefficients. The highlight of this expression is the presence of the 6th order term, introduced to account for the existence of a crossover from a second order to a first order transition with a concomitant tricritical point TCP[23]. Minimisation of eq. (2) yields

$$\theta = \left[R\left(1+\frac{3t}{t_0}\right)^{1/2} - 1 \right]^{1/2}, \quad \text{where } R = b/3c \tag{3}$$

In this model t_0 is an all important parameter, describing the crossover temperature at which the behaviour changes from mean field like to tricritical like; the nearer the value is to zero, closer it is to the TCP with $t_0 = 0$ occuring at the tricritical point. As the bulk sample exhibits a weak first order transition with a consequential jump in the tilt angle, its data is not fitted to eq. (3). An attempt to do so will lead to very small values of t_0, apparently indicating that the system lies very close to TCP. In contrast, the smooth variation of θ with temperature for the Anopore sample makes it a better candidate to perform such a fitting. The fitting of the Anopore data to eq. (3) is shown in Figure 11 (b). The value of t_0 obtained (0.003, see Table 2), indicates that the transition is a second-order one and quite far away from TCP. These results suggest that confinement has transformed the nature of the transition from first order to second order.

The temperature variation of the dielectric constant perpendicular to the director ($\varepsilon_\perp$) at different fixed frequencies for the bulk sample is shown in Figure 12 (a). For the measuring frequency of 0.1 and 1 kHz, the onset of the SmA-SmC* transition is marked by a large increase in the $\varepsilon_\perp$ value. The large magnitude of $\varepsilon_\perp$ in the SmC* phase is expected for this compound with high spontaneous polarisation. When the frequency is increased, although the qualitative behaviour remains the same, there is a substantial decrease in the value. With a further increase in frequency to 100 kHz, the behaviour also changes, having a peak-like appearance at the transition. The features seen in the SmC* phase at low frequencies suggest the presence of a significantly active Goldstone mode having a relaxation frequency in the range of 1–10 kHz. The peaking of the data at 100 kHz is indicative of the soft mode arising out of tilt fluctuations. Across the SmC*-CrG transition, $\varepsilon_\perp$ drops to quite low values even at low frequencies. The thermal variation of $\varepsilon_\perp$ for Anopore sample is shown in Figure 12 (b) [For the bulk sample, $\varepsilon_\perp$ is determined using the standard equation for parallel plate capacitor. For the Anopore sample $\varepsilon_\perp$ is calculated using the relation $\varepsilon_\perp = (C_{obs} - C_{Matrix})/C_{air}$, where C_{Matrix} is the capacitance of empty Anopore membrane. Using the relation $C_{Matrix} = \varepsilon_0 A(\varepsilon_{Matrix} + \varepsilon_{air})/d$, ε_{Matrix} is calculated.]. The most significant feature to be noticed is that in the SmC* phase the maximum value of $\varepsilon_\perp$ is much smaller than the value obtained for the bulk sample. However, the thermal variation is quite similar to that seen for the bulk sample at low frequencies. These two aspects indicate the presence of a partially suppressed Goldstone mode, owing to a possible partial unwinding of the helix driven by the narrow pore size.

The relaxation parameters were determined by analyzing the frequency dependent spectrum of the dielectric constant using the Havriliak-Negami function. It is now well established that the collective relaxation in these systems can be analyzed in terms of the fluctuations of the two component tilt order parameter[24]. The amplitude part of the tilt gives rise to the soft mode (SM), which softens on approaching the transition from either of the phases. The azimuthal angle part is responsible for the Goldstone mode (GM), which is active only in the SmC* phase. The temperature dependence of f_R and $\Delta\varepsilon$ for the bulk and Anopore samples are shown in Figures 13(a) and 13(b) respectively. For the bulk sample, as the transition is approached from the SmA phase the observed decrease in f_R and the concomitant increase in $\Delta\varepsilon$, is a feature characteristic of the soft mode. At the transition GM appears, and due to its overwhelming dielectric strength the soft mode is hardly observed in the SmC* phase. For the Anopore sample, the behaviour in the SmA phase is identifiable with the one observed for the bulk sample, namely that the relaxation frequency decreases as the transition is approached, while the dielectric strength increases. The magnitude of the relaxation frequency is, however, different. For example, at $T_C + 1°C$, the f_R value for the Anopore sample is about 2.5 times higher than that for the bulk. The rate at which f_R decreases on approaching T_C is also more for the Anopore (374 kHz/°C) than for the bulk (295 kHz/°C). It is interesting to see that this rate for the the Anopore sample is comparable to that obtained (363 kHz/°C) when a DC bias field, known to unwind the helix, is applied to the bulk sample. This feature supports our argument that the confinement results in the unwinding of the helix. In the SmC* phase only one mode is observed, whose relaxation frequency lies in the range of 600 kHz. Although one may like to ascribe such a high frequency relaxation with the soft mode, the temperature-independent nature of f_R and the associated $\Delta\varepsilon$ precludes such an interpretation. In fact, the trend seen suggests the behaviour of GM. However, it should be noted that

Figure 12: Temperature variation of the dielectric constant perpendicular to the director ($\varepsilon_\perp$) in the (a) bulk and (b) Anopore configurations for the A7 sample, measured at four different fixed frequencies. The sharp increase and the precipitous drop seen at low frequencies at the SmA–SmC* and SmC*–CrG transitions are as expected. The much smaller value for the Anopore sample is argued to be due to the partial suppression of the Goldstone mode.

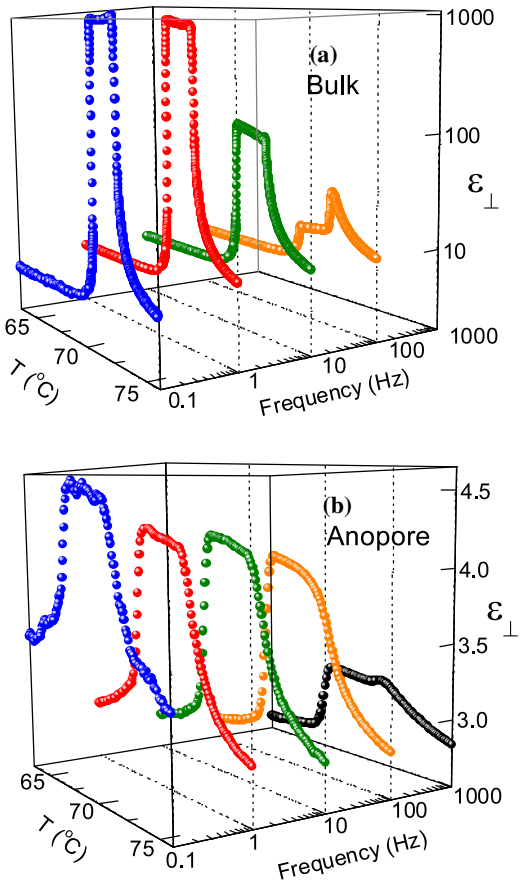

these f_R values are about 400 times larger than the GM of the bulk sample. But to be noted is the point that in the presence of a bias field the value of GM increases by about an order of magnitude for the bulk sample. Therefore we associate the relaxation mode seen in the SmC* phase to that of the GM, but with a substantially unwound helix. The reason for the unwinding is the comparable magnitude of the helical pitch with the pore diameter and the interaction of the liquid crystalline molecules with the walls of the confining membrane.

4.2. *TCOB*

The overall change in the d value is quite small across the SmA-SmC transition in the bulk and Anopore geometries (Figure 14). The minimal layer shrinkage seen, as quantified by the ratio of $d_c/d_A = 0.98$ (d_A is taken just at T_c and d_c at $T_c - 10°C$), puts the SmA phase of this material in the class of de Vries SmA. Upon confinement in the Anopore membrane the qualitative behaviour is the same as that for the bulk sample but with an increased absolute value in the SmC, as seen in other cases mentioned above. The total change across the transition is smaller and smeared out for the Anopore sample. The smearing also observed for another material (8OSI*: see Figure 15) and the A7 compound discussed above, appears to be a general feature for the SmA-SmC transition upon confinement irrespective of the magnitude of the change in d across the transition. Also seen in each of these cases is that in the SmA phase before the transition there is a slight downward trend in the d value as the temperature is decreased. It is possible that the anchoring at the Anopore surface provides a "pre-tilt" even in the SmA phase, and if true, the transition would correspond to a change from a low tilt to a high tilt phase. Such an effect, seen in the

Figure 13: Dependence of the relaxation frequency (f_R, red set) and the dielectric strength ($\Delta\varepsilon$, blue set) on reduced temperature, $T_c - T$ (T_c being the transition temperature) for the (a) bulk and (b) Anopore samples in the compound A7.

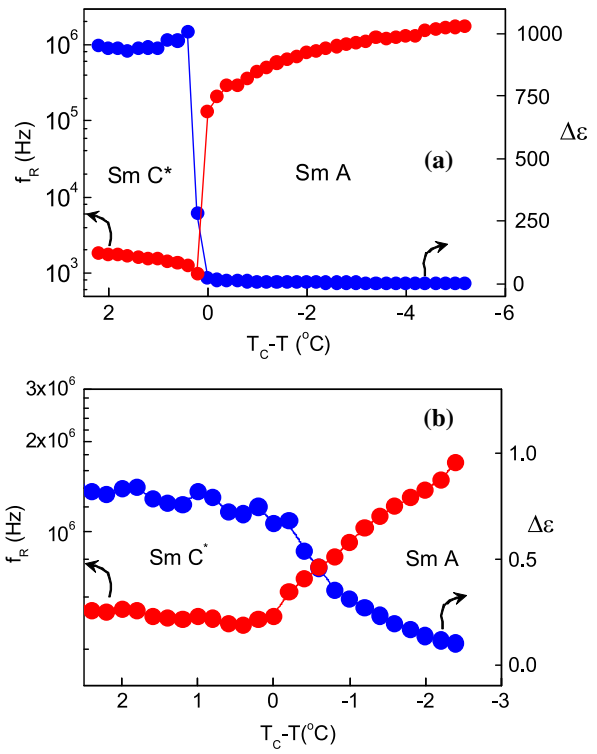

case of electric field induced changes, would actually break the symmetry of the SmA phase, making the phases across the transition isosymmetric with important consequences. Experiments to explore this possibility would be interesting.

Determining the tilt angle in the SmC phase as described for the A7 compound and fitting the temperature-dependent data for 8OSI* to eq. (3) we get the parameters t_o and R, which are tabulated in Table 2 (The tilt angle data for the TCOB sample confined in the Anopore membrane had a linear variation with temperature, unlike the parabolic dependence for the other two samples. Thus no fitting was done to the TCOB data). Notice that for both A7 and 8OSI*, confinement increases the value of t_o: effectively the system moves further away from TCP (Bulk A7 has a first order transition and therefore t_o is not defined. However, since moving towards a second order transition upon confinement would require a crossing-over through a TCP having $t_o = 0$, this statement is justified.). Thus the effect of confinement seems to reduce the influence of the TCP on the order parameter variation. This view is corroborated by the ratio of b/c, which gives the relative influence of the TCP on the mean field behaviour of the system: b is small and c large close to TCP ($b = 0$ at TCP); when confined, b/c increases. Whereas b/c increases by 6.7 times between the bulk and Anopore 8OSI* systems, the derived ratio b/a also increases by approximately the same value (6.3), suggesting that it must be the enhancement of b that is responsible for the observed behaviour. Then, t_o should increase by a factor of square of b/c, which is indeed the case as seen in Table 2.

A feature to be noted in the data for TCOB is that in the SmA phase, away from the transition to the SmC phase, d increases with decreasing temperature and in the vicinity of the transition (at a temperature marked T_1 in figure 14) shows a plateau before exhibiting a smooth drop at T_c, the transition temperature. Such a result first seen by us[25] in a system with partially bilayer SmA and SmC phases, was recently observed[26] in a chiral material with minimal layer shrinkage. The authors of the latter report argue that T_1 marks a transition between a conventional SmA (at high temperature) to a de Vries SmA phase. While this aspect seen for both the bulk and Anopore samples of TCOB could be associated with such a crossover transition, an equally possible argument is the following. 8OSI*

Figure 14: Thermal variation of the layer spacing d across the SmA-SmC transition of the de Vries compound TCOB in bulk (blue circles) and Anopore (red circles) geometries. Notice that the transition is smeared out for the Anopore sample. While T_c is the transition temperature, the meaning of T_1 is discussed in the text.

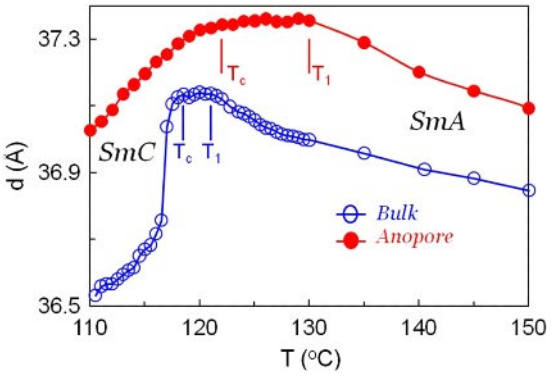

Figure 15: Temperature dependence of the layer spacing d across the SmA-SmC* transition of the compound 8OSI* in the bulk and Anopore geometries, showing a substantial change in the d value, as is expected for a non-de Vries material. To demonstrate the existence of plateau-like region, argued[26] to be due to de Vries situation, but seen for 8OSI* also, the data in the bulk geometry is shown on an enlarged scale in the inset.

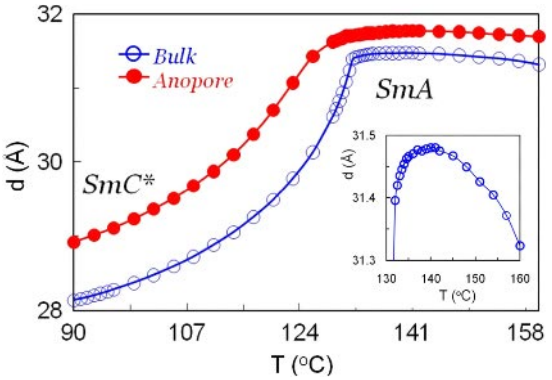

has a large variation of d across the SmA-SmC* transition and thus cannot be termed as a de Vries material. The inset of figure 15 shows on an enlarged scale, the temperature variation of d in the SmA phase for 8OSI*. Note that there appears to be a crossover behaviour similar to the ones seen for the de Vries materials mentioned above. Therefore we suggest that the change of slope in the thermal variation of d in the SmA phase may not be associated with an additional transition. A possible alternative explanation[14] could be the following. The large increase in d with decreasing temperature in the SmA phase is due to the thermally driven stretching of the alkyl chains. Below T_c, the tendency of the molecules to tilt with respect to the layer normal results in a decrease in the layer spacing. Thus in the temperature range between T_c and T_1, the competition between the two opposing trends could lead to the observation of a plateau region. This would mean that the effect at T_1 is only an artifact and not due to any thermodynamic phase transition. This is perhaps the reason Huang et al[26] did not observe any calorimetric signature at T_1.

4.3. *Influence of confinement on the thermodynamics of phase transitions*

A general trend that has been observed is that as the pore size of the confining medium decreases the transition enthalpy decreases. Dadmun and Muthukumar[27] have attempted to give an explanation for the lowering of transition temperatures as well as transition enthalpies on

Table 3: Thompson length β and the interface energy σ values for 4OBC and 4O.8 compounds confined in Anopore membranes

Compound	Phase	β(nm)	$\sigma(10^{-3}$ J/m$^2)$
4OBC	Melting (Cr-HexB)	3.44	15.5
	HexB-SmA	0.57	0.25
	SmA-I	0.49	2.89
4O.8	CrB-SmA	0.56	0.49
	N-I	1.37	0.1

the basis of surface anchoring and finite size effects. According to this argument small finite clusters undergo the transition at a temperature lower than that in the bulk owing to the fact that clusters (or domains) could be poorly correlated. Melting in pores does not differ fundamentally from melting of free particles in a strongly disperse state and in both cases the process can be regarded as the size effect[28]. The presence of curved pore surface may only facilitate breakdown of the long-range positional order and in the limiting case of a monolayer it can result in complete absence of such order. The formation of small crystals was first theoretically described by Gibbs[29]. The related theory for the effect of curvature on the vapour pressure of liquid droplets was derived by Thomson[30]. The actual expression used to estimate ΔT_m, the depression in the melting point of substances in confined geometries, often called the Gibbs-Thomson equation, is given by

$$\Delta T_m = T_m - T_m^R = \frac{2T_m \Delta\sigma}{\Delta H_m \rho R} \qquad (4)$$

Here T_m and T_m^R stand for the melting point of the sample in bulk and confined states, $\Delta\sigma$ is the surface tension difference between the solid and liquid phases, ΔH_m is the bulk enthalpy of fusion, ρ is the mass density of the sample and R is the radius of the pore. In the case of the N-I transition, this expression has been employed to estimate either $\Delta\sigma$ or using known value of $\Delta\sigma$ to compare with the experimentally determined depression in the transition temperature when the material is confined in porous media. For the cyano biphenyl compounds, using the experimentally reported values of $\Delta\sigma$[31] it was found that the calculated value of T_m is at least an order of magnitude smaller than that actually observed.

Table 3 lists the Thompson length β and the interface energy σ values determined using eq. (5) for the compounds 4O.8 and 4OBC used in this study. Considering the fact that the value of $\Delta\sigma$ is about the same for different materials, the shift in the N-I transition temperature for 4O.8 supports the above mentioned argument. Further it is also noticed that surface tension measurements on one of the compounds used by us, viz., 4O.8, did not show any noticeable change across the SmA–CrB transition[32], whereas our thermal investigations have shown a reduction in the transition temperature for the Anopore samples. Thus it can be safely concluded that at least in liquid crystalline systems surface tension effects alone cannot explain the magnitude of the shift in the transition temperature. The first feature to be noted is that the value of the Thompson length β $(=4\sigma/\Delta H_m \rho)$, defined as the thickness of the interface layer, depends on the type of phase transition, having the highest value for the crystal melting (Cr-HexB) transition and least for the N-I transition. These values are much higher compared to the Thompson length for the melting transition of non-liquid crystalline materials, especially water for which $\beta = 0.15$ nm[33]. At least, for the first order transition (transitions except Sm-A-Hex-B in the present case) it means that the size of the nuclei formed is much larger than in the case of crystallization of water. The value of σ for the melting of 4OBC is of the same order as that for 5CB[28]. The value for the N-I transition of 4O.8 is in agreement with that for 5CB[28]. Although the bulk enthalpies of SmA-I and melting transitions are comparable, the interface energy is much higher for the former.

Another mechanism that has been considered for the shift in the transition temperature is based on the following view. With respect to the molecules at the boundary of the pores, the liquid crystalline molecules in the bulk (well inside the pores) must arrange themselves to minimize the elastic energy caused by surface forces at the walls. A simple-minded argument that takes into account such a feature leads to $\Delta T_m = 4\pi^2$ K$_o/2a_o R^2$, where K_o is the Frank elastic constant and a_o is the usual Landau-de Gennes coefficient. This expression yields ΔT values of $\sim$ 1 k, in good agreement with the experiments.

Acknowledgments

We sincerely appreciate the participation of the students Dr. Chethan Vishal Lobo and Dr. K.L. Sandhya, and Dr. Anjuli Khandelwal, Physics Department, S.D. (P.G) College, Muzaffarnagar in this programme. Partial financial support from the U.S. Office of Naval Research (ONR Grant No. N00014-97-1-0904) under an Indo-US collaborative program is gratefully acknowledged.

Received 28 January 2009.

References

1. K. M. Unruh, T. E. Huber, C. A. Huber Phys. Rev. B **48**, 9021 (1993)

2. L. D. Gelb, K. E. Gubbins, R. Radhakrishnan and M. Sliwinska-Bartkowiak Rep. Prog. Phys. **62**, 1573 (1999); R. Radhakrishnan, K. E. Gubbins and M. Sliwinska-Bartkowiak, J. Chem. Phys. **116**, 1147 (2002).
3. J. Klein and E. Kumacheva, Science, **269**, 816 (1995).
4. I. Rhee, F. M. Gasparini and D. J. Bishop, Phys. Rev. Lett., **63**, 410 (1989).
5. D. Murphy, E. Genio, G. Ahlers, F. Liu, and Y. Liu, Phys. Rev. Lett., **90**, 025301 (2003).
6. M. Arndt, R. Stannarius, H. Groothues, E. Hempel and F. Kremer, Phys. Rev. Lett., **79**, 2077 (1997).
7. R. Zorn, L. Hartmann, B. Frick, D. Richter and F. Kremer, J. Non-Crys. Solids, **307–310**, 547 (2002).
8. See e.g., Liquid Crystals in Complex Geometries. Eds: Crawford G. P. and Zumer S. (London: Taylor & Francis) (1996).
9. G. S. Iannacchione, Fluid Phase Equilibria, **222–223**, 177 (2004).
10. M. Vilfan, I. D. Olenik and M. Copic, in "Time-resolved spectroscopy in complex liquids: an experimental perspective ", Ed. R. Torre, Springer 2008
11. K. L. Sandhya, Geetha G. Nair, S.Krishna Prasad and Anjuli Khandelwal, Liq. cryst., **28**, 1847 (2001).
12. K. L. Sandhya, S. Krishna Prasad, D. S. Shankar Rao and Ch. Bahr, Phys. Rev. E, 66, 031710 (2002).
13. Chethan V. Lobo, S. Krishna Prasad, and D. S. Shankar Rao, Phys. Rev. E, 69, 051706 (2004).
14. Chethan V. Lobo, S. Krishna Prasad, and D. S. Shankar Rao, Phys. Rev. E, 72, 062701 (2005).
15. Chethan V. Lobo, S. Krishna Prasad, and C. V. Yelamaggad, J. Phys Condens. Matter, **18**, 767 (2006).
16. V. Jayalakshmi, Geetha G. Nair and S. Krishna Prasad, J. Phys Condens. Matter, 19, 226213 (2007).
17. S. Chandrasekhar, "Liquid Crystals", (Cambridge University Press, 1992).
18. For a summary on this topic see W. H. de Jeu, B. I. Ostrovskii and A. N. Shalaginov. Rev. Mod. Phys. 75, 181 (2003)
19. G. Aeppli and R. Bruinsma, Phys. Rev. Lett. **53**, 2133 (1984).
20. S. C. Davey, J. Budai, J. W. Goodby, R. Pindak, and D. E. Moncton, Phys. Rev. Lett. **53**, 2129 (1984); T. Pitchford, G. Nounesis, S. Dumrongrattana, J. M. Viner, C. C. Huang, and J. W. Goodby, Phys. Rev. A **32**, 1938(1985).
21. A. de Vries, Mol. Cryst. Liq. Cryst. **41**, 27 (1977); see also N. A. Clark, T. Bellini, R.-F. Shao, D. Coleman, S. Bardon, D. R. Link, J. E. Maclennan, X.-H. Chen, M. D. Wand, D. M. Walba, P. Rudquist, and S. T. Lagerwall, Appl. Phys. Lett. 80, 4097 (2002).
22. C. C. Huang and J. M. Viner, Phys. Rev. A 25, 3385 (1982).
23. R. Shashidhar, B. R. Ratna, Geetha G. Nair, S. Krishna Prasad, Ch. Bahr and G. Heppke, Phys. Rev. Lett., 61, 547(1988).
24. T. Carlsson, B. Zeks, C. Filipic and A. Levstik, Phys. Rev. A 42, 877 (1990).
25. S. Krishna Prasad, D. S. Shankar Rao, V. N. Raja, S. Chandrasekhar, G. Heppke and M. E. Neubert, Mol. Cryst. Liq. Cryst., 238, 241 (1994).
26. C. C. Huang, S. T. Wang, X. F. Han, A. Cady, R. Pindak, W. Caliebe, K. Ema, K. Takekoshi, and H. Yao, Phys. Rev. E, 69, 041702 (2004).
27. M. D. Dadmun and M. Muthukumar, J. Chem. Phys., **98**, 4850 (1993).
28. F. M. Aliev and N. Breganov, Sov. Phys. JETP, 68, 70 (1989).
29. J. W. Gibbs, Collected works, Vol.1, Yale University Press, New Haven 1928.
30. W. Thomson (Lord Kelvin), Philos. Mag., 42, 448 (1871).
31. M. G. J. Gannon and T. E. Faber, Phil. Mag., 37, 117 (1978); also see S. Krishna Swamy, Ph.D thesis, Mysore University (1983).
32. K. Miyano, Phys. Rev. A, 26, 1820 (1982).
33. J. Rault, R. Neffati and P. Judeinstein, Eur. Phys. J. B., 36, 627 (2003).

S. Krishna Prasad is a scientist at the Centre for Liquid Crystal Research, Bangalore. His current research activities include photo-stimulated phenomena and Transitions in restricted geometries of soft matter, especially liquid crystals.

D. S. Shankar Rao is working as a scientist at the Centre for Liquid Crystal Research, Jalahalli, Bangalore. His research interests include phase transition, critical phenomena, etc in liquid crystals.

Geetha G. Nair is a scientist at the Centre for Liquid Crystal Research, Bangalore. Her research interests include photo-induced phase transitions in liquid crystals, rheological studies of soft materials such as liquid crystalline gels.